Journal of Zhejiang University-SCIENCE A (Applied Physics & Engineering)
ISSN 1673-565X (Print); ISSN 1862-1775 (Online)
www.zju.edu.cn/jzus; www.springerlink.com
E-mail: jzus@zju.edu.cn

# Strain transfer of surface-bonded fiber Bragg grating sensors for airship envelope structural health monitoring*

Hai-tao ZHAO†, Quan-bao WANG, Ye QIU†‡, Ji-an CHEN, Yue-ying WANG, Zhen-min FAN

(*School of Aeronautics and Astronautics, Shanghai Jiao Tong University, Shanghai 200240, China*)

†E-mail: zht@sjtu.edu.cn; qiuye@sju.edu.cn

Received Dec. 10, 2011; Revision accepted May 3, 2012; Crosschecked May 29, 2012

**Abstract:** This paper deals with an improved bonding approach of surface-bonded fiber Bragg grating (FBG) sensors for airship envelope structural health monitoring (SHM) under the strain transfer theory. A theoretical formula is derived from the proposed model to predict the strain transfer relationship between the airship envelope and fiber core. Then theoretical predictions are validated by numerical analysis using the finite element method (FEM). Finally, on the basis of the theoretical approach and numerical validation, parameters that influence the strain transfer rate from the airship envelope to fiber core and the ratio of effective sensing length are analyzed, and some meaningful conclusions are provided.

**Key words:** Airship envelope, Fiber Bragg grating (FBG), Surface-bonded, Strain transfer, Structural health monitoring (SHM)
**doi:**10.1631/jzus.A1100336 **Document code:** A **CLC number:** V27

## 1 Introduction

Airships have a great potential for different purposes such as regional disaster prevention, environmental monitoring, urban security, missile defense, regional communications, and so on (Colozza and Dolce, 2005). The inflatable body, which generates the lift, is the core structure of an airship (Wang *et al.*, 2009). Strain monitoring of the inflatable body (i.e., the airship envelope) is of great importance to ensure the safety of the airship structures. Airship structural health monitoring (SHM) using optical fiber sensors, for instance, fiber Bragg grating (FBG) sensors, is a new and functional concept during the airship development from a low-level airship to stratospheric one. Qiu *et al.* (2012) investigated the feasibility of FBG-based SHM for ZHIYUAN-1 airship (Fig. 1) nosecone qualitatively and put forward some technical proposals. In order to ensure the smooth operation of the whole structures of airships, strain monitoring of airship envelopes is another significant aspect. However, up to date and to the best knowledge of the authors, there is limited research on FBG-based airship envelope SHM, and research in this area is warranted due to the multitude of functionalities which airships are capable of fulfilling.

On the other hand, in recent years, FBG sensors have been a reliable monitoring tool and the first choice among optical fiber sensors applied in SHM due to their inherent advantages of being lightweight with small dimensions, fast responsiveness, immunity to electromagnetic interference, resistance to corrosion, etc. (Betz *et al.*, 2006). For FBG-based airship envelope SHM, one of the key technologies is the study of strain transfer characteristics of surface-bonded FBG sensors. Since airship envelopes are membrane structures, a surface-bonded type is the primary approach to integrate FBGs with them. As a strain sensor, it is expected that the strains between the fiber core and airship envelope are the same (Duck *et al.*, 1999). However, due to the existence of an adhesive layer and coating material (such as

‡ Corresponding author
* Project (No. 2011AA7052011) supported by the National High-Tech R&D (863) Program of China

**Fig. 1 ZHIYUAN-1 airship manufactured by Shanghai Jiao Tong University, China**

polymer that protects the fiber core due to its brittle performance), where part of the energy is converted into their shear deformations, a strain inconsistency between the fiber core and airship envelope remains (Cheng *et al*., 2010). For FBG sensors, the influence of strain inconsistency is apparent and could not be neglected since FBGs serve as short gauge optical fiber sensors. In order to improve the accuracy of strain measurement of FBG sensors, the influence of the coating and adhesive layer should be taken into consideration to modify the strain value measured by the fiber core. While, most researchers have focused on the theoretical study of strain transfer characteristics of embedded FBG sensors, research on surface-bonded types is still not sufficient. A main reason is that the asymmetry of surface-bonded FBG structures brings in increased difficulty for mechanical analysis. Cheng *et al.* (2005) developed an analytic model of a bonding layer for an FBG model bonded on a host material and predicted the strain transfer from host material to FBG when the host material is subjected to external forces. Wan *et al.* (2008) established a 3D-finite element method (FEM) to simulate the strain transfer of a surface-bonded optical fiber sensor and investigated the influence of geometric parameters of the adhesive layer on the strain transfer. Her and Huang (2011) established a model of a surface-bonded optical fiber sensor and evaluated the interaction between the host material and coating. The above three analytic models mainly target the strain monitoring of rigid host materials. The bonding approaches of Cheng *et al.* (2005) and Her and Huang (2011) could not properly maintain the bonding stability between FBG and the airship envelope (Fig. 2a and Fig. 2c). Wan *et al.* (2008) wrapped the entire FBG to form a circular bonding layer and solved the problem of stability; while the shape and width of adhesive layer would not correspond to actual demand in the case of airship envelopes (Fig. 2b). In consideration of the structural characteristics of airship envelopes, it is necessary to improve the analytic model of surface-bonded FBG (mainly referring to the bonding approach) to predict the strain transfer rate from the airship envelope to the fiber core so as to accord with the actual situation.

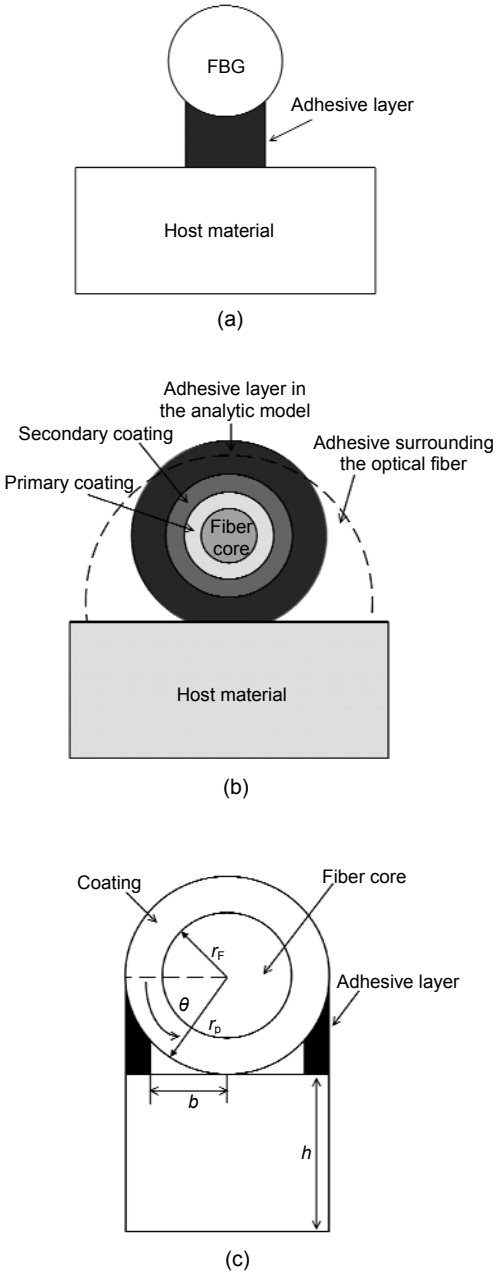


**Fig. 2 Surface-bonded FBG models of Cheng *et al.* (2005) (a), Wan *et al.* (2008) (b), and Her and Huang (2011) (c)**

In this paper, based on the three bonding approaches of the above models, we propose an improved surface-bonded FBG model that is suitable for airship envelope SHM. A theoretical formula is derived from the proposed model to predict the strain transfer relationship between the airship envelope and the fiber core. Then, a numerical simulation by the FEM is conducted to validate theoretical predictions. Finally, parameters of the adhesive layer (width, Young's modulus, top and bottom thickness) that influence the strain transfer rate from the airship envelope to fiber core are analyzed, which provides a design reference for airship envelope SHM in future research and practice.

## 2 Theoretical approach

The improved surface-bonded FBG model is shown in Fig. 3a and Fig. 3b, and the stress distribution of the longitudinal section is shown in Fig. 3c. An external axial load is applied to airship envelope. The deformation of the fiber core induced by the airship envelope is transferred through adhesive layer and coating, which induces a change in optical signal transfer (Song *et al.*, 2004). Strain transfer characteristics between the airship envelope and surface-bonded FBG are derived based on the following assumptions (Pak, 1992; Ansari and Libo, 1998; Zhou *et al.*, 2010):

1. Materials of all parts including the fiber core, coating and airship envelope behave as linear elastic isotropic materials. The airship envelope under the bonding portion is approximately flat and behaves as homogeneous strain along the fiber.

2. Only the airship envelope is subjected to uniform axial stress, whereas the fiber core, coating and adhesive layer do not bear any external loadings directly.

3. All the interfaces are perfectly bonded so that the displacements are consistent along the interfaces.

In this analysis, the subscripts F, C, A and H, respectively represent the physical quantities related to the fiber core, coating, adhesive layer and airship envelope. $E$, $G$ and $\lambda$ denote Young's modus, shear modulus and Poisson's ratio, respectively. $u$ and $w$ are the axial displacement and radial displacement, respectively. $\sigma$, $\tau$, $\varepsilon$, and $\gamma$ are the axial stress, shear stress, strain and shear strain, respectively. $L_F$, $h_A$ and $W_A$ are half of the bonding length of FBG, top thickness of adhesive layer and width of adhesive layer, respectively. $r$ denotes the spatial variable that is the coordinate along the radial of the center of the optical fiber.

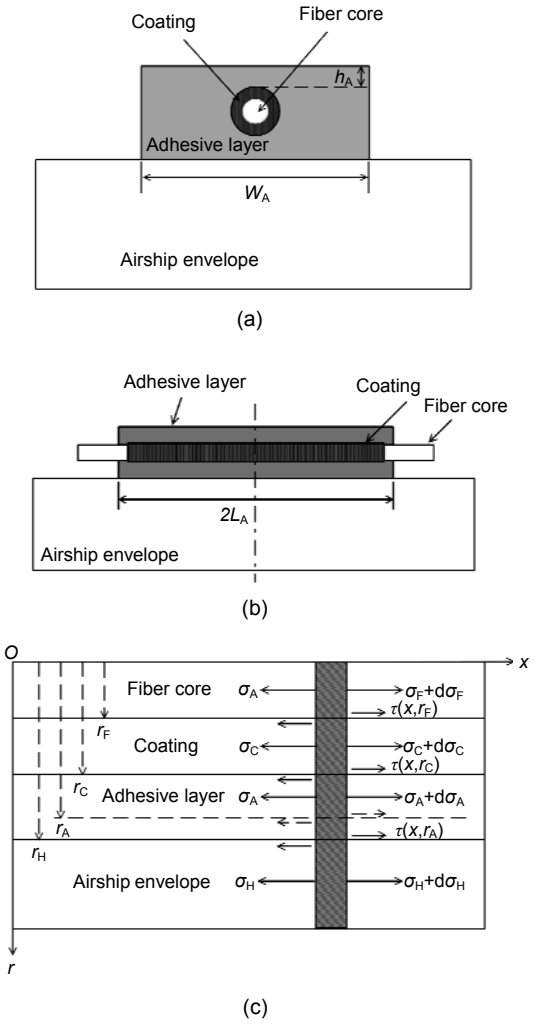


**Fig. 3 Improved analytic model of surface-bonded FBG sensor for airship envelope SHM**

Cross section (a), longitudinal section (b), and stress distribution of the longitudinal section (c) of the surface-bonded FBG model

Under the assumptions 1–3, the equilibrium equation for infinitesimal fiber core is

$$\pi r_F^2 \sigma_F = \pi r_F^2 (\sigma_F + \mathrm{d}\sigma_F) + 2\pi r_F \tau(x, r_F)\mathrm{d}x, \qquad (1)$$

where

$$\frac{\mathrm{d}\sigma_{\mathrm{F}}}{\mathrm{d}x}=-\frac{\tau(x,r_{\mathrm{F}})}{r_{\mathrm{F}}}. \tag{2}$$

Similarly, the equilibrium equation for infinitesimal coating and adhesive layer are, respectively:

$$\frac{\mathrm{d}\sigma_{\mathrm{C}}}{\mathrm{d}x}=\frac{2[r_{\mathrm{F}}\tau(x,r_{\mathrm{F}})-r_{\mathrm{C}}\tau(x,r_{\mathrm{C}})]}{r_{\mathrm{C}}^2-r_{\mathrm{F}}^2}, \tag{3}$$

$$\frac{\mathrm{d}\sigma_{\mathrm{A}}}{\mathrm{d}x}=\frac{2\pi r_{\mathrm{C}}\tau(x,r_{\mathrm{C}})-\tau(x,r)W_{\mathrm{A}}}{W_{\mathrm{A}}(h_{\mathrm{A}}+r_{\mathrm{C}}+r)-\pi r_{\mathrm{C}}^2}. \tag{4}$$

By Eqs. (2)–(4) we can obtain:

$$\begin{aligned}\tau(x,r)=&-\frac{2\pi r_{\mathrm{F}}^2}{W_{\mathrm{A}}}\frac{\mathrm{d}\sigma_{\mathrm{F}}}{\mathrm{d}x}+\frac{\pi(r_{\mathrm{F}}^2-r_{\mathrm{C}}^2)}{W_{\mathrm{A}}}\frac{\mathrm{d}\sigma_{\mathrm{C}}}{\mathrm{d}x}\\&-\left(h_{\mathrm{A}}+r_{\mathrm{C}}+r-\frac{\pi r_{\mathrm{C}}^2}{W_{\mathrm{A}}}\right)\frac{\mathrm{d}\sigma_{\mathrm{A}}}{\mathrm{d}x}.\end{aligned} \tag{5}$$

When the stress transfers between host material and optical fiber, the shear modulus of deformation is dominant and the radial deformation of optical fiber is secondary. Therefore, the Poisson effect could be ignored. Substituting the equation $\sigma=E\varepsilon$ into Eq. (6), where $\varepsilon=\dfrac{\mathrm{d}u}{\mathrm{d}x}$ denotes the axial strain and $u=u(x)$ indicates the displacement, yields:

$$\begin{aligned}\tau(x,r)=&-\frac{2\pi r_{\mathrm{F}}^2E_{\mathrm{F}}}{W_{\mathrm{A}}}\frac{\mathrm{d}\varepsilon_{\mathrm{F}}}{\mathrm{d}x}+\frac{\pi(r_{\mathrm{F}}^2-r_{\mathrm{C}}^2)E_{\mathrm{C}}}{W_{\mathrm{A}}}\frac{\mathrm{d}\varepsilon_{\mathrm{C}}}{\mathrm{d}x}\\&-\left(h_{\mathrm{A}}+r_{\mathrm{C}}+r-\frac{\pi r_{\mathrm{C}}^2}{W_{\mathrm{A}}}\right)E_{\mathrm{A}}\frac{\mathrm{d}\varepsilon_{\mathrm{A}}}{\mathrm{d}x}\\=&E_{\mathrm{F}}\left[-\frac{2\pi r_{\mathrm{F}}^2}{W_{\mathrm{A}}}\frac{\mathrm{d}\varepsilon_{\mathrm{F}}}{\mathrm{d}x}+\frac{\pi(r_{\mathrm{F}}^2-r_{\mathrm{C}}^2)E_{\mathrm{C}}}{W_{\mathrm{A}}E_{\mathrm{F}}}\frac{\mathrm{d}\varepsilon_{\mathrm{C}}}{\mathrm{d}x}\right.\\&\left.-\left(h_{\mathrm{A}}+r_{\mathrm{C}}+r-\frac{\pi r_{\mathrm{C}}^2}{W_{\mathrm{A}}}\right)\frac{E_{\mathrm{A}}}{E_{\mathrm{F}}}\frac{\mathrm{d}\varepsilon_{\mathrm{A}}}{\mathrm{d}x}\right].\end{aligned} \tag{6}$$

As the fiber core deforms synchronously with the other layers, the strain gradients of all the layers are approximately the same, i.e.,

$$\frac{\mathrm{d}\varepsilon_{\mathrm{C}}}{\mathrm{d}x}\cong\frac{\mathrm{d}\varepsilon_{\mathrm{A}}}{\mathrm{d}x}\cong\frac{\mathrm{d}\varepsilon_{\mathrm{F}}}{\mathrm{d}x}. \tag{7}$$

Substituting Eq. (7) into Eq. (6) yields:

$$\begin{aligned}\tau(x,r)=&\left[-\frac{2\pi r_{\mathrm{F}}^2E_{\mathrm{F}}}{W_{\mathrm{A}}}-\frac{\pi(r_{\mathrm{F}}^2-r_{\mathrm{C}}^2)E_{\mathrm{C}}}{W_{\mathrm{A}}}\right.\\&\left.-\left(h_{\mathrm{A}}+r_{\mathrm{C}}+r-\frac{\pi r_{\mathrm{C}}^2}{W_{\mathrm{A}}}\right)E_{\mathrm{A}}\right]\frac{\mathrm{d}\varepsilon_{\mathrm{F}}}{\mathrm{d}x}.\end{aligned} \tag{8}$$

Since the FBG sensors possess a large aspect ratio, the radial displacement could be ignored, i.e.,

$$\tau(x,r)=G_{\mathrm{A}}\gamma(x,r)=G_{\mathrm{A}}\left(\frac{\partial u}{\partial r}+\frac{\partial w}{\partial x}\right)\cong G_{\mathrm{A}}\frac{\mathrm{d}u}{\mathrm{d}r}. \tag{9}$$

Substituting Eq. (9) into Eq. (8) and integrating Eq. (8) from ($r_{\mathrm{F}}$, $r_{\mathrm{H}}$) leads to:

$$\begin{aligned}\int_{r_{\mathrm{F}}}^{r_{\mathrm{H}}}\left(G_{\mathrm{A}}\frac{\mathrm{d}u}{\mathrm{d}r}\right)\mathrm{d}r=&-\int_{r_{\mathrm{F}}}^{r_{\mathrm{H}}}\left[\frac{2\pi r_{\mathrm{F}}^2E_{\mathrm{F}}}{W_{\mathrm{A}}}+\frac{\pi(r_{\mathrm{F}}^2-r_{\mathrm{C}}^2)E_{\mathrm{C}}}{W_{\mathrm{A}}}\right.\\&\left.+\left(h_{\mathrm{A}}+r_{\mathrm{C}}+r-\frac{\pi r_{\mathrm{C}}^2}{W_{\mathrm{A}}}\right)E_{\mathrm{A}}\frac{\mathrm{d}\varepsilon_{\mathrm{F}}}{\mathrm{d}x}\right]\mathrm{d}r,\end{aligned} \tag{10}$$

and yields:

$$\begin{aligned}u_{\mathrm{H}}-u_{\mathrm{F}}=&-\frac{r_{\mathrm{H}}-r_{\mathrm{F}}}{W_{\mathrm{A}}G_{\mathrm{A}}}\left\{2\pi r_{\mathrm{F}}^2E_{\mathrm{F}}+\pi(r_{\mathrm{F}}^2-r_{\mathrm{C}}^2)E_{\mathrm{C}}\right.\\&\left.+\left[W_{\mathrm{A}}\left(h_{\mathrm{A}}+r_{\mathrm{C}}+\frac{r_{\mathrm{F}}}{2}+\frac{r_{\mathrm{H}}}{2}\right)-\pi r_{\mathrm{C}}^2\right]\right\}\frac{\mathrm{d}\varepsilon_{\mathrm{F}}}{\mathrm{d}x}\\=&-\frac{1}{k^2}\frac{\mathrm{d}\varepsilon_{\mathrm{F}}}{\mathrm{d}x}.\end{aligned} \tag{11}$$

Thus, we can obtain:

$$k=\sqrt{\frac{W_{\mathrm{A}}G_{\mathrm{A}}}{(r_{\mathrm{H}}-r_{\mathrm{F}})\left\{2\pi r_{\mathrm{F}}^2E_{\mathrm{F}}+\pi(r_{\mathrm{F}}^2-r_{\mathrm{C}}^2)E_{\mathrm{C}}+\left[W_{\mathrm{A}}\left(h_{\mathrm{A}}+r_{\mathrm{C}}+\frac{1}{2}r_{\mathrm{F}}+\frac{1}{2}r_{\mathrm{H}}\right)-\pi r_{\mathrm{C}}^2\right]E_{\mathrm{A}}\right\}}}, \tag{12}$$

where $k$ is the strain lag parameter containing the effects of the fiber core, coating and adhesive layer. Differentiating Eq. (11) with respect to $x$, yields:

$$\frac{\mathrm{d}^2\varepsilon_{\mathrm{F}}(x)}{\mathrm{d}x^2}-k^2\varepsilon_{\mathrm{F}}(x)=-k^2\varepsilon_{\mathrm{H}}. \tag{13}$$

The general solution of Eq. (13) is

$$\varepsilon_{\mathrm{F}}(x)=C_1\mathrm{e}^{kx}+C_2\mathrm{e}^{-kx}+\varepsilon_{\mathrm{H}}, \tag{14}$$

where $C_1$ and $C_2$ are the integration constants that are determined by boundary conditions.

The fiber core is assumed free from axial stress at both ends, and the boundary condition is given by

$$\varepsilon_{\mathrm{F}}(L_{\mathrm{F}})=\varepsilon_{\mathrm{F}}(-L_{\mathrm{F}})=0. \tag{15}$$

Thus, $C_1$ and $C_2$ can be evaluated by imposing the boundary condition on Eq. (13) and obtained as

$$C_1=C_2=-\frac{\varepsilon_{\mathrm{H}}}{2\cosh(kL_{\mathrm{F}})}, \tag{16}$$

The final solution to Eq. (13), i.e., the strain relationship of the fiber core to airship envelope is

$$\varepsilon_{\mathrm{F}}(x)=\varepsilon_{\mathrm{H}}\left(1-\frac{\cosh(kx)}{\cosh(kL_{\mathrm{F}})}\right). \tag{17}$$

The maximum strain transfer rate $\psi_{\mathrm{m}}(0)$ happens at the midpoint of the fiber core (i.e., the point where $x$ is equal to zero), and yields to:

$$\psi_{\mathrm{H}}(0)=\frac{\varepsilon_{\mathrm{F}}(0)}{\varepsilon_{\mathrm{H}}}=1-\frac{1}{\cosh(kL_{\mathrm{F}})}. \tag{18}$$

Normally, the strain measured by FBG sensor is the average strain over the bonding length of FBG. Average strain transfer rate $\overline{\psi}$ can be expressed as

$$\overline{\psi}=\frac{\overline{\varepsilon_{\mathrm{F}}(x)}}{\varepsilon_{\mathrm{H}}}=\frac{2\int_0^L\varepsilon_{\mathrm{F}}(x)\mathrm{d}x}{2L_{\mathrm{F}}\varepsilon_{\mathrm{H}}}=1-\frac{\sinh(kL_{\mathrm{F}})}{kL_{\mathrm{F}}\cosh(kL_{\mathrm{F}})}. \tag{19}$$

Through the whole analysis, it validated that Eqs. (12) and (18) can be used to calculate the strain transfer rate of a surface-bonded FBG sensor used for airship envelope SHM.

## 3 Numerical validation and parameter analysis

### 3.1 Numerical validation

In this section, a numerical simulation is carried out using commercial software ANSYS Workbench to validate the theoretical predictions. Geometric and mechanic parameters of FBGs are considered as known quantities, which are listed in Table 1. Other desired parameters (mainly associating with the parameters of the adhesive layer and airship envelope) are assigned in Table 2. In order to improve the calculation efficiency of the computer, the airship envelope is assumed to be the same length and width as the adhesive layer. In addition, since the model is a symmetrical structure, we select the left half of the structure as the analytic model.

**Table 1 Known quantities of the FBG model**

| Parameter | Value |
|---|---|
| Young's modulus of fiber core, $E_{\mathrm{F}}$ (Pa) | $7.2\times10^{10}$ |
| Poisson's ratio of fiber core, $\lambda_{\mathrm{F}}$ | 0.17 |
| Outer radius of fiber core, $r_{\mathrm{F}}$ (mm) | 0.0625 |
| Young's modulus of coating, $E_{\mathrm{C}}$ (Pa) | $2.55\times10^{6}$ |
| Poisson's ratio of coating, $\lambda_{\mathrm{C}}$ | 0.48 |
| Outer radius of coating, $r_{\mathrm{C}}$ (mm) | 0.1025 |

**Table 2 Assigned quantities of the FBG model**

| Parameter | Value |
|---|---|
| Top thickness of adhesive layer, $h_{\mathrm{A}}$ (mm) | 0.05 |
| Bottom thickness of adhesive layer, $r_{\mathrm{H}}$–$r_{\mathrm{C}}$ (mm) | 0.07 |
| Width of adhesive layer, $W_{\mathrm{A}}$ (mm) | 0.80 |
| Young's modulus of adhesive layer, $E_{\mathrm{A}}$ (Pa) | $4\times10^{9}$ |
| Poisson's ratio of adhesive layer, $\lambda_{\mathrm{A}}$ | 0.34 |
| Half of the bonding length of FBG, $L_{\mathrm{F}}$ (mm) | 30 |
| Young's modulus of airship envelope, $E_{\mathrm{H}}$ (Pa) | $3\times10^{8}$ |
| Poisson's ratio of airship envelope ($\lambda_{\mathrm{H}}$) | 0.35 |
| Thickness of airship envelope, $W_{\mathrm{H}}$ (mm) | 0.1 |

Fig. 4 shows the finite element meshes of the analytic model. An axial load of 50 N is applied to the end of the airship envelope. The axial strain

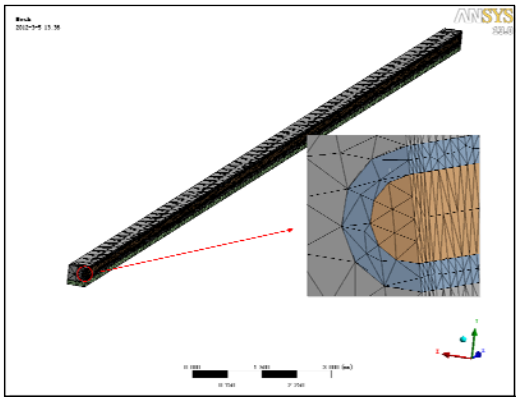

**Fig. 4 Finite element meshes**

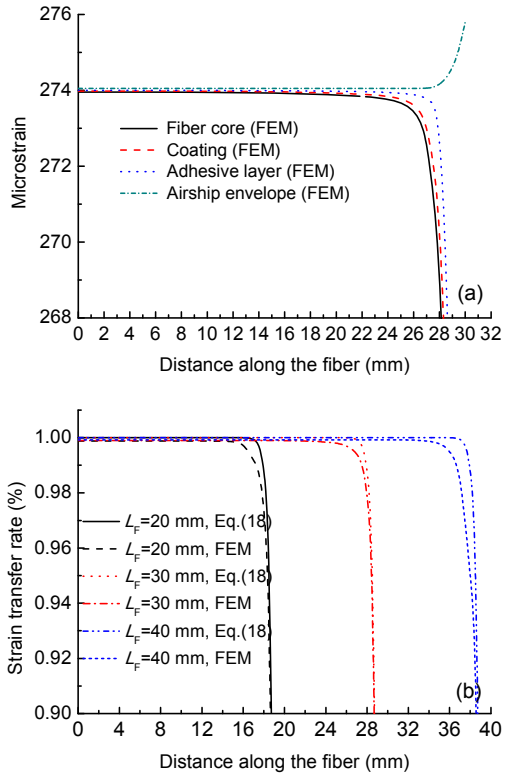


**Fig. 5 FEM results**

(a) Axial strain distribution of each layer by the FEM; (b) Comparison of the axial strain distribution along the fiber by the FEM and Eq. (18)

distribution of each layer by the FEM is shown in Fig. 5a. It clearly indicates that the axial strain of each layer is non-uniform along the fiber and changes rapidly in the position of half bonding length $L_F$> 24 mm. The axial strains of the airship envelope and other layers change conversely. We can also find that the strain of each layer at the mid-beam region (half bonding length $L_F$≤24 mm) is approximately equal; while, the strain inconsistency manifests itself between the layers when half bonding length $L_F$> 24 mm. Fig. 5b illustrates the axial strain transfer rate along the fiber with different half bonding lengths, which is obtained by the FEM and Eq. (17) respectively as a comparison. It is shown that theoretical predictions are in good agreement with the FEM results.

### 3.2 Parametric analysis

Since FBG sensors widely serve as commercially available products, parameters of the fiber core and coating are considered as known quantities (Table 1) and are not taken into consideration in the parameter analysis (Zhou *et al.*, 2006). Therefore, relevant parameters of adhesive layer are the primary object to analyze the impact factors on strain transfer rate.

Assigned parameter values of the FBG sensor are: half bonded length $L_F$=30 mm, width of adhesive layer $W_A$=0.8 mm, Young's modulus of adhesive layer $E_A$=4×10$^9$ Pa, Poisson's ratio of adhesive layer $\lambda_A$=0.34, top thickness of adhesive layer $h_A$=0.05 mm, and bottom thickness of adhesive layer $r_H$−$r_C$= 0.07 mm. Fig. 6a shows the strain transfer rate along the fiber with different widths of adhesive layer. The ratio of the effective sensing length ascends with the increase of the width of adhesive layer; Fig. 6b shows the strain transfer rate along the fiber with different top thickness of adhesive layer. The ratio of the effective sensing length descends with the increase of the top thickness of adhesive layer; Fig. 6c shows the strain transfer rate along the fiber with different bottom thickness of adhesive layer. The ratio of the effective sensing length descends with the increase of the bottom thickness of adhesive layer; Fig. 6d shows the strain transfer rate along the fiber with different Young's modulus of adhesive layer. The ratio of the effective sensing length ascends with the increase of the Young's modulus of adhesive layer.

As can be seen from the four figures, the width, bottom thickness and Young's modulus of the adhesive layer are important impact factors on the strain transfer rate and the ratio of effective sensing length. While, the influence of top thickness of the adhesive layer on the strain transfer rate and the ratio of the effective sensing length is negligible.

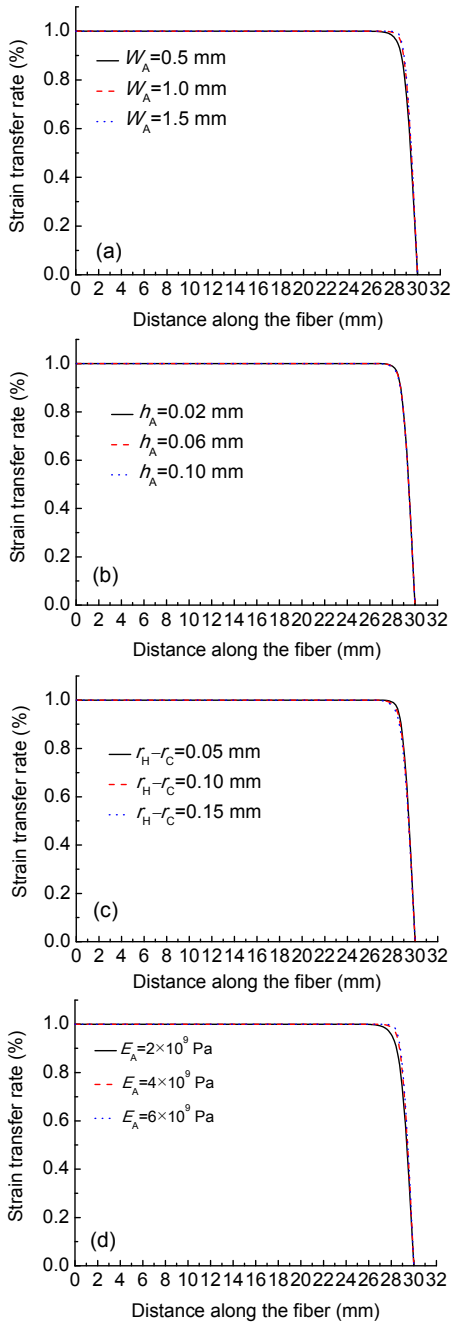


**Fig. 6 Parametric analysis results**

Strain transfer rate along the fiber with different widths of the adhesive layer $W_A$ (a), different top thickness of the adhesive layer $h_A$ (b), different bottom thickness of the adhesive layer $r_H$−$r_C$ (c), and different Young's modulus of the adhesive layer $E_A$ (d)

## 4 Conclusions

In this paper, an improved surface-bonded FBG strain transfer model for airship envelope SHM is proposed with a theoretical formula to predict the strain transfer relationship between the airship envelope and fiber core. Theoretical predictions are validated by a numerical analysis using FEM. Based on the theoretical approach and numerical validation, geometric and mechanic parameters of adhesive layer that influence the strain transfer rate and the ratio of effective sensing length are analyzed. Results show that the width and Young's modulus are the most critical parameters; while the impacts of bottom thickness and Poisson's ratio are slight and minimal. Conclusions from this study provide a design reference for future research on airship envelope SHM.

## References

Ansari, F., Libo, Y., 1998. Mechanics of bond and interface shear transfer in optical fiber sensors. *Journal of Engineering Mechanics*, **124**(4):385-394. [doi:10.1061/(ASCE)0733-9399]

Betz, D.C., Thursby, G., Culshaw, B., Staszewski, W.J., 2006. Advanced layout of a fiber Bragg grating strain gauge rosette. *Journal of Lightwave Technology*, **24**(2):1019-1026. [doi:10.1109/JLT.2005.862442]

Cheng, C.C., Lo, Y.L., Pun, B.S., Chang, Y.M., Li, W.Y., 2005. An investigation of bonding-layer characteristics of substrate-bonded fiber Bragg grating. *Journal of Lightwave Technology*, **23**(11):3907-3915. [doi:10.1109/JLT.2005.856235]

Cheng, C.C., Lo, Y.L., Li, W.Y., 2010. Accurate simulations of reflective wavelength spectrum of surface-bonded fiber Bragg grating. *Applied Optics*, **49**(17):3394-3402. [doi:10.1364/AO.49.003394]

Colozza, A., Dolce, J.L., 2005. High-Altitude, Long-Endurance Airships for Coastal Surveillance. NASAPTM-2005-213427.

Duck, G., Renaud, G., Measures, R., 1999. The mechanical load transfer into a distributed optical fiber sensor due to a linear strain gradient: embedded and surface bonded cases. *Smart Materials and Structures*, **8**(2):175-181. [doi:10.1088/0964-1726/8/2/002]

Her, S.C., Huang, C.Y., 2011. Effect of coating on strain transfer of optical fiber Bragg sensors. *Sensors*, **11**(7):6926-6941. [doi:10.3390/s110706926]

Pak, Y.E., 1992. Longitudinal shear transfer in fiber optic sensors. *Smart Materials and Structures*, **1**(1):57-62. [doi:10.1088/0964-1726/1/1/008]

Qiu, Y., Wang, Q.B., Zhao, H.T., Chen, J.A., 2012. Applications of FBG Sensors for Airship Structural Health Monitoring. The Fourth IEEE International Symposium on Photonics and Optoelectronic (SOPO), Shanghai, China, in press.

Song, I.C., Lee, S.K., Jeong, S.H., Lee, B.H., 2004. Absolute strain measurements made with fiber Bragg grating sensors. *Applied Optics*, **43**(6):1337-1341. [doi:10.1364/

AO.43.001337]

Wan, K.T., Leung, C.K.Y., Olson, N.G., 2008. Investigation of strain transfer for surface-attached optical fiber strain sensors. *Smart Materials and Structures*, **17**(3):035037. [doi:10.1088/0964-1726/17/3/035037]

Wang, Q.B., Chen, J.A., Fu, G.Y., Duan, D.P., 2009. An approach for shape optimization of stratosphere airship based on multidisciplinary design optimization. *Journal of Zhejiang University SCIENCE-A*, **10**(11):1609-1616. [doi:10.1631/jzus.A0820814]

Zhou, G.D., Li, H.N., Ren, L., Li, D.S., 2006. Influencing Parameters Analysis of Strain Transfer in Optic Fiber Bragg Grating Sensors. Proceedings of SPIE, **6179**: 6179R.

Zhou, J., Zhou, Z., Zhang, D., 2010. Study on strain transfer characteristics of fiber Bragg grating sensors. *Journal of Intelligent Material Systems and Structures*, **21**(11):1117-1122. [doi:10.1177/1045389X10375997]